Numerical simulations of thermal convection in unsteady Darcy Forchheimer flow of radiative $Ag - GO/KO$ hybrid nanofluid over a slipping spinning porous disk

Zahoor Iqbal [a,b], Farhan Ali [e], Huiying Xu [a,*], Xinzhong Zhu [a,c,d,**], M.M. Alqarni [f], Arafat Hussain [g], Sharifah E. Alhazmi [h], Ehab M. Ragab [i], M. Faizan Ahmed [e]

[a] School of Computer Science and Technology, Zhejiang Normal University, Jinhua, 321004, China
[b] Zhejiang Institute of Photoelectronics & Zhejiang Institute for Advanced Light Source, Zhejiang Normal University, Jinhua, Zhejiang, 321004, China
[c] Research Institute of Hangzhou Artificial Intelligence, Zhejiang Normal University, Hangzhou, Zhejiang, 311231, China
[d] College of Computer Science and Artificial Intelligence, Wenzhou University, Wenzhou 325035, China
[e] Department of Mathematical Sciences, Federal Urdu University of Arts, Sciences and Technology, Gulshan-e-Iqbal Karachi, 75300, Pakistan
[f] Department of Mathematics, College of Sciences, King Khalid University, Abha, 61413, Saudi Arabia
[g] College of Mathematics and System Science, Xinjiang University, Urumqi, Xinjiang, China
[h] Mathematics Department, Al-Qunfudah University College, Umm Al-Qura University, Mecca, USA
[i] Department of Civil Engineering, Engineering College, Northern Border University, Arar, Saudi Arabia

A R T I C L E   I N F O

A B S T R A C T

The thermal transport in hybrid nanofluid flow across a rotating disk has numerous applications in technical and engineering fields, including thermal power systems, rotating machinery, gas turbines, and electronics. The Hybrid nanofluids offer better thermal efficiency than traditional single-component nanofluids due to the inclusion of two types of metallic nanoparticles. This study examines the thermal behavior of an $Ag - GO/KO$ hybrid nanofluid flowing over a rotating, slippery disk under a highly oscillating magnetic field. The model incorporates a thermal sink/source and thermal radiation to enhance its applicability in practical scenarios. The Tiwari and Das approach is used to examine the characteristics of the fluid flow. The model equations are obtained by applying the proper Von-Karman similarity transformations to the strongly non-linear system of governing equations, which is then numerically solved using the bvp4c technique in MATLAB. The effects of physical parameters on thermal field, radial velocity, axial velocity, and tangential direction are visually displayed. The findings indicate that a rise in the inertia coefficient and porosity variable leads to produce a reducing effect on the radial velocity and tangential velocity. In contrast, the opposite impact is examined in the axial direction. Additionally, the result demonstrates the improved temperature distribution due to higher thermal radiation and unsteady variable. Moreover, tables are depicted to numerically discuss the impacts of slip variables, heat radiation and unsteady variables on drag coefficients and heat transport.

---

* Corresponding author.
** Corresponding author. School of Computer Science and Technology, Zhejiang Normal University, Jinhua, 321004, China.
  E-mail addresses: xhy@zjnu.edu.cn (H. Xu), zxz@zjnu.edu.cn (X. Zhu).

1. Introduction

A rotating system has proved the subject of extensive investigation in the past few years. It has developed popularity amongst academics because of its numerous applications. Medical equipment, rotating wind turbines, heating and cooling systems, and crystal development procedures are just a few of the industrial and aviation science fields in which it finds use. Von Kármán [1] discussed the continuous rotational movement caused near a spinning disk. This kind of movement includes a circumferential gradient of pressure across the disk, that optimizes the forces of centrifugal force. Nadeem et al. [2] described the second law analysis on the heat radiation and heat sink/source in the presence of inertia coefficient due to rotating disk. Nayak et al. [3] explained the axisymmetric rotating flow of Darcian Forchheimer due to stretchable/shrinkable nanofluid due to rotating disk. Chu et al. [4] described the dual stability of stagnation of Darcian Forchheimer due to a rotating disk. Umavathi et al. [5] examined the slip effect of nanoliquid using Darcian Forchheimer flow past a rotating. Sharma et al. [6] studied the machine learning approach on the hybrid nanofluid due to a rotating disk with a chemical reaction. Ali et al. [7] simplified the influence of convective of CMC-water base hybrid nanofluid past a rotating disk. Nisar et al. [8] explored the magneto signal nanofluid using ethylene glycol and water due to stretchable disks.

Recent advancements in nanomaterials have drawn a lot of interest from scientists and researchers because of its vast economic and scientific implications. Many of the uses of nanotechnology have been brought to the actual world since its inception. Choi [9] first noted that introducing tiny nanoparticles with high thermal conductivity properties could increase the energy transport capacity (thermal conductivity) of ordinary fluids. Abedel et al. [10] scrutinized the impact of heat radiation of nanofluid past a stretchable sheet in the presence of Darcy Forchheimer flow. Moreover, Cui et al. [11] carried out the thermal analysis on the Darcy Forchheimer heat radiation across oblique sheet. The thermal analysis of heat radiation from chemical reactions in nanofluids caused by stretchy sheets was discovered by Nisar et al. [12]. Haider et al. [13] explored the effect of variable viscosity on the nanofluid past a stretchable sheet induced by Dacry Forchheimer. The impact of the porous material of the magneto flow chemically reactive nanofluid with heat radiation was examined by Nisar et al. [14]. Through the chemical reactive process, Eswaramoorthi et al. [15] investigated the ohmic heating with thermal radiation for the CNT nanofluid. Using machine learning, Habib et al. [16] investigated how nanoliquid affected chemically reactive substances. The importance of Darcian Forchheimer in the SWCNT of a single nanofluid beyond a stretched sheet while taking thin film flow into consideration was described by Nisar et al. [17]. The inclined magnetic flow of thin film for the nanofluid with nonlinear mixed convective was described by Saeed et al. [18]. The combined impact of heat radiation and source on a viscoelastic nanofluid in the presence of activation energy was described by Dharmaiah et al. [19].

Simultaneous mixing or ultrasonication can be used to create bi-hybrid, as the base fluid's thermal properties are enhanced by adding one or more nanoscale particles. Nanofluids have garnered significant interest from researchers over the past decade. The broad range of industrial applications for kerosene oil-based nanofluids includes heat transfer systems, combustion engines, oil refineries, renewable energy systems, and more. Kerosene oil is combined with various types of nanoparticles to optimize heat transfer and reduce energy loss within the system. To recognize this, Ahmad et al. [20] conducted a theoretical analysis on the kerosene oil-based hydromagnetic hybrid nanofluid past surface expanding in the presence of energy source, and convective constraints. The implications of suction and slip conditions over the hydromagnetic motion of Maxwell tri-hybrid nano-liquid over an enlarging sheet with activation energy were analysed by Hussain et al. [21]. They observed that, the Nusselt number exhibits a dominant trend with a greater Hartmann parameter. Zeeshan et al. [22] studied the various shape factor effects of copper nanoparticles on the steady transport of water-based nano-fluid on stretching and rotating disks. Nisar et al. [23] computed the thermal analysis of trihybrid nanofluid induced by the Lorentz dipole through nonlinear heat radiation. Alnahdi et al. [24] described the novel features of tri-hybrid nanofluid through a couple of stresses in a channel. Nisar et al. [25] explained the significance of couple stress on the time-dependent flow of hybridized viscous nanofluid through the gyrating sphere. Behrouz et al. [26] examined the thermophysical characteristics of hybridized nanofluid with chemically reactive. Dinarvand et al. [27] discussed the shape factor with heat source across an inclined magnetic field for the hybrid nanofuid in the squeezing flow. Berreh et al. [28] carried out the irreversible analysis on the hybrid nanofluid with convective flow past a movable wedge. Dinarvand [29] talked about the consequent of micropolar mixed convective flow of hybrid nanofluid.

The term 'porous media' refers to materials that contain voids or pores, which offer resistance to fluid flow. Porous media are commonly used to control heat transfer and regulate fluid velocity in various industrial processes, such as hazardous material disposal and oil extraction. High-velocity flow problems are modelled using the modified Darcy-Forchheimer equation, although the fundamental Darcy law still applies to understanding the properties of these materials. Applications involving porous media flow are primarily found in drying processes, material processing, cellular technologies, and oil extraction. An energy transmission analysis of the Darcy-Forchheimer electromagnetic transport of ethylene glycol-based nanofluid over a rotating cone placed on an expandable disk was presented by Al-Arabi et al. [30]. Alhadri et al. [31] performed the neural networking-based computations for the water-based hybrid hydromagnetic nano liquid past an expandable surface under the impacts of suction and ohmic heating. The influence of the porous magnetic flow of binary chemical reaction with chemical reaction was demonstrated by Nisar et al. [32]. The solar thermal absorption analysis of magnetohydrodynamic flow phenomena involving a Newtonian nanofluid with an energy source was conducted by Alzahrani et al. [33]. Ali et al. [34] conducted the concentration and thermal analysis of hybrid nanofluid in a porous medium due accelerated exponential vertical sheet. The axisymmetric flow of MHD CNT caused by a stretchable sheet with heat radiation was identified by Nisar et al. [35].

Generally, Velocity slip, which is the term for the phenomenon when a fluid fails to cling to a solid barrier, has been seen in specific situations. When a fluid, such as an emulsion, suspension, foam, or polymer solution, is particulate, a velocity slip may happen on the extending border. Boundary slip-exhibiting fluids find significant technical uses, including internal cavities and prosthetic heart valve polishing. Navier's slippage condition, where the rate of slip velocity relates to the localized shear stress, replaces the no-slip condition

for some covered surfaces, like Teflon, that resist stickiness. The stability analysis on the hydromagnetic hybrid nano liquid slip flow of carbon nanotubes over an enlarging medium with an energy source was performed by Lund et al. [36]. The outcomes of velocity slip and radiative heat flux on the hydromagnetic water-based nano liquid over a stretching disk with entropy creation were discussed by Acharya et al. [37]. Rahman and Eltayeb [38] analysed the influence of temperature-dependent properties on the convective slip flow of a Newtonian fluid over a stretching wedge with variable viscosity.

The magneto flow of a radiative flow hybrid nanofluid $(GO + AG/KO)$ over a porous spinning disk under slip conditions has not been studied. The aforementioned question and thorough review of the research literature show that while many papers have been written about nanofluids with different geometric shapes, there is less information available about hybrid nanofluids that use a revolving disk and a base fluid of kerosene oil (KO). This study intends to optimize grease, improve surface properties, and enable effective catalysis for real-world applications in tribology research, power systems, automobile engines, and substance coatings.

In accordance with the literature review above, the focus of current work is to analyse the spinning Darcy Forchheimer slip flow due to a rotating disk for the time-dependent hybrid nanofluid $(GO + AG/KO)$ inside a thermal radiation and magnetic field. The non-linear partial differential equations are governed through mathematical modelling. Applying similarity transformation technique, a set of ordinary differential equations is obtained. Finally, Bvp4c method is applied to address the resulting equations. The influence of multiple factors on radial velocity, tangential velocity, heat rate, axial velocity, skin friction factor, and thermal profiles are examined with the aid of graphs and tables. The unique characteristics of silver and graphene oxide provide a combination of improved physical performance, chemical resistance, and interaction with the surface that is appropriate to use in grease, catalysts, and surface engineering. Ag-GO/KO was selected due to its ability to address practical issues associated with friction decrease, wear avoidance, modification of the surface, and catalytic efficiency.

2. Mathematical Formulation

Consider a Darcy Forchheimer flow of time-dependent radiative $Ag - GO/KO$ hybrid nano-fluid towards a slippery spinning disk. The disk is moving with angular velocity speed $\frac{\omega}{(1-\gamma t)}$ about the z-axis, where $1 - \gamma t > 0$ represents the unsteady state and γ is a positive constant. The cylindrical coordinate (r, Φ, z) with velocity component (u, v, w) in which the disk is positioned next to $z = 0$ and half space of the disk is filled through the hybrid nanofluid. For hybrid nanoparticles, Ag and GO are suggested. The fluid is dispersed over $z \geq 0$ and the spinning disc is positioned at $z = 0$. T_∞ represents ambient temperature, while the disc surface consumes a uniform temperature of T_w as described in Fig. 1. With these assumptions, system's leading models of the flow are listed below:

The model equations has been given below [2–4].

$$\frac{u}{r} + \frac{\partial u}{\partial r} + \frac{\partial w}{\partial z} = 0 \tag{1}$$

$$u = \frac{\delta \omega r}{(1-\gamma t)} + L u_z, \quad v = \frac{\omega r}{(1-\gamma t)} + L u_z, \quad w = 0, T = T_w$$
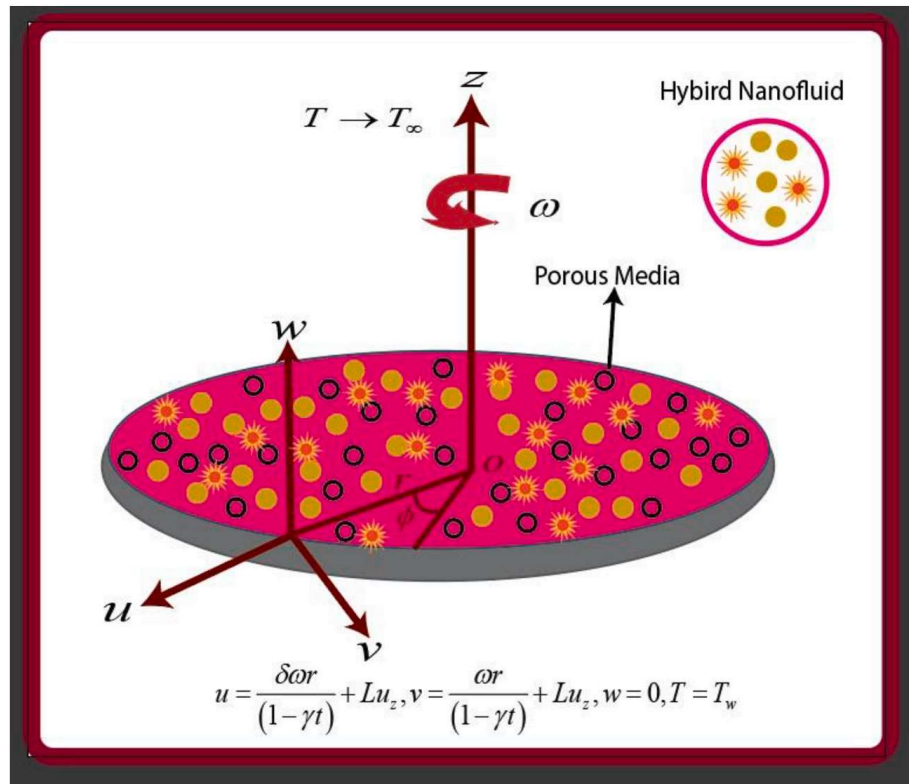
Fig. 1. Physical model of Darcian Forchheimer Hybrid nanofluid.

$$\left(\frac{\partial u}{\partial t}+u\frac{\partial u}{\partial r}+w\frac{\partial u}{\partial z}-\frac{v^2}{r}\right)=-\frac{1}{\rho_{hnf}}\frac{\partial p}{\partial r}+\frac{\mu_{hnf}}{\rho_{hnf}}\left(\frac{\partial^2 u}{\partial r^2}+\frac{\partial^2 u}{\partial z^2}+\frac{1}{r}\frac{\partial u}{\partial r}-\frac{u}{r^2}\right)-F_0 u^2-\frac{\mu_{hnf}}{K\rho_{hnf}}u, \tag{2}$$

$$\left(\frac{\partial v}{\partial t}+u\frac{\partial v}{\partial r}+w\frac{\partial v}{\partial z}+\frac{uv}{r}\right)=\frac{\mu_{hnf}}{\rho_{hnf}}\left(\frac{\partial^2 v}{\partial r^2}+\frac{\partial^2 v}{\partial z^2}+\frac{1}{r}\frac{\partial v}{\partial r}-\frac{v}{r^2}\right)-F_0 v^2-\frac{\mu_{hnf}}{K\rho_{hnf}}v \tag{3}$$

$$\left(u\frac{\partial w}{\partial r}+w\frac{\partial w}{\partial z}\right)=\frac{\mu_{hnf}}{\rho_{hnf}}\left(\frac{\partial^2 w}{\partial r^2}+\frac{\partial^2 w}{\partial z^2}+\frac{1}{r}\frac{\partial w}{\partial r}\right)-\frac{1}{\rho_{hnf}}\frac{\partial p}{\partial r} \tag{4}$$

$$\frac{\partial T}{\partial t}+u\frac{\partial T}{\partial r}+w\frac{\partial T}{\partial z}=\left(\frac{16T_\infty^3\sigma^*}{3k_{hnf}(\rho C_p)_{hnf}}+\frac{k_{hnf}}{(\rho C_p)_{hnf}}\right)\left[\frac{\partial^2 T}{\partial r^2}+\frac{1}{r}\frac{\partial T}{\partial r}+\frac{\partial^2 T}{\partial z^2}\right]+\frac{Q^*}{(\rho C_p)_{hnf}}(T-T_\infty), \tag{5}$$

2.1. Thermophysical properties

In this simulation, the base fluid is kerosene oil (*KO*). Silver oxide and graphene oxide (*GO*) are selected as nanoparticles to create the hybrid nanosuspension. For the mono nanofluid, only graphene oxide (*GO*) is added. The thermophysical properties of nanoparticles in the base fluid are displayed in Table 1. By setting the second particle concentration value (Φ_2) to zero, the results for the mono nanofluid are obtained. This study is conducted for both mono and hybrid nanofluids, which have been displayed in Table 2.

The boundary conditions in the appropriate form are given below:

$$u=\frac{\delta\omega r}{(1-\gamma t)}+Lu_z, v=\frac{\omega r}{(1-\gamma t)}+Lv_z, w=0, T=T_w \text{ at } z=0$$

$$u\to 0, v\to 0, T\to T_\infty \text{ at } z\to\infty \tag{6}$$

Where $L=L'\sqrt{1-\gamma t}$ and γ is the stretching factor.

To convert the equations into dimensionless form, below similarity variables are applied:

$$\xi=\sqrt{\frac{\omega}{\nu_f(1-\gamma t)}}z, u=\frac{rw}{(1-\gamma t)}F(\xi), v=\frac{rw}{(1-\gamma t)}G(\xi), w=\sqrt{\frac{\nu_f\omega}{(1-\gamma t)}}H(\xi), \Xi(\xi)=\frac{T-T_\infty}{T-T_w} \tag{7}$$

By applying a transformation (6) over equations (1)–(4), the system is expressed in the following dimensionless form:

$$2F+H'=0, \tag{8}$$

$$F''-\frac{\Omega_1}{\Omega_2}\left\{F^2-G^2+HF'+\gamma\left(F+\frac{\xi}{2}F'\right)\right\}-\frac{\Omega_1}{\Omega_2}FrF^2-\alpha_1 F=0, \tag{9}$$

$$G''-\frac{\Omega_1}{\Omega_2}\left\{2FG+HG'+\gamma\left(G+\frac{\xi}{2}G'\right)\right\}-\frac{\Omega_1}{\Omega_2}FrG^2-\alpha_1 F=0, \tag{10}$$

$$\left(\Omega_4+\frac{4}{3}Rd\right)\Xi''-\Omega_3 Pr\left(H\Xi'+\gamma\frac{1}{2}\Xi'\right)=0, \tag{11}$$

Where, $\Omega_2=\frac{\rho_{hnf}}{\rho_f}, \Omega_3=\frac{(\rho c_p)_{hnf}}{(\rho c_p)_f}, \Omega_4=\frac{k_{hnf}}{k_f}, \Omega_1=\frac{\mu_{hnf}}{\mu_f}$,

The boundary conditions shown equation (5) also transformed by using transformation technique (6). Finally, below boundary conditions are obtained:

$$F(0)=\Gamma+\Pi F'(0), F(\infty)=0, G(0)=1+\Pi G'(0),$$

$$G(\infty)=0, H(0), \Xi(0)=1, \Xi(\infty)=0 \tag{12}$$

Table 1
Thermophysical properties of nanoparticles and base fluid [39].

	KO	*GO*	*Ag*
ρ	783	1800	10500
k	0.145	5000	429
C_p	2090	717	235
σ	21×10^{-6}	6.30×10^7	63×10^{-6}
Shape	–	Spherical	Spherical
Size(nm)	–	2	0.144

Table 2
Thermophysical model for ($GO + Ag$).

Properties	AG/KO
Density (ρ)	$\frac{\rho_{nf}}{\rho_f} = (1 - \Upsilon_1) + \frac{\Upsilon_1 \rho_{1s}}{\rho_f}$
Viscosity(μ)	$\frac{\mu_{nf}}{\mu_f} = \frac{1}{(1 - \Upsilon_1)^{2.5}}$
Thermal conductivity (k)	$\frac{k_{nf}}{k_f} = \frac{k_1 + 2k_f - 2\Upsilon_1(k_f - k_1)}{k_1 + 2k_f + \Upsilon_1(k_f - k_1)}$
Heat Capacity (ρC_p)	$\frac{(\rho c_p)_{nf}}{(\rho c_p)_f} = (1 - \Upsilon_1) + \frac{\Upsilon_1(\rho c_p)_{1s}}{(\rho c_p)_f}$
Properties	**AG + GO/KO**
Density (ρ)	$\frac{\rho_{hnf}}{\rho_f} = (1 - \Upsilon_1)\left[(1 - \Upsilon_2) + \frac{\Upsilon_2 \rho_{2s}}{\rho_f}\right] + \frac{\Upsilon_1 \rho_{1s}}{\rho_f}$
Viscosity(μ)	$\frac{\mu_{hnf}}{\mu_f} = \frac{1}{(1 - \Upsilon_1)^{2.5}(1 - \Upsilon_2)^{2.5}}$
Thermal conductivity (k)	$\frac{k_{hnf}}{k_f} = \frac{k_{s1} + 2k_{hnf} - 2\Upsilon_1(k_{hnf} - k_1)}{k_{s1} + 2k_{hnf} + \Upsilon_1(k_{hnf} - k_1)} \times \frac{k_{s2} + 2k_{nf} - 2\Upsilon_2(k_{nf} - k_{s2})}{k_{s2} + 2k_{nf} + \Upsilon_2(k_{nf} - k_{s2})} k_f$
Heat Capacity (ρC_p)	$\frac{(\rho c_p)_{hnf}}{(\rho c_p)_f} = (1 - \Upsilon_1)\left[(1 - \Upsilon_2) + \frac{\Upsilon_2(\rho c_p)_{2s}}{(\rho c_p)_f}\right] + \frac{\Upsilon_1(\rho c_p)_{1s}}{(\rho c_p)_f}$

2.2. Physical quantities

The main engineering quantities of interest are Nusselt number and frictional parameter defined as follows:

$$Cf_r = \frac{1}{\rho_{hnf}\left(\frac{r\omega}{1-\gamma t}\right)^2}\sqrt{\tau_{wr} + \tau_{w\phi}}, Nu_r = \frac{rq_w}{k_f(T_w - T_\infty)} \tag{13}$$

$$\tau_{wr} = \mu_{hnf}\left(\frac{\partial u}{\partial z} + \frac{\partial w}{\partial r}\right)_{z=0}, \tau_{w\phi} = \mu_{hnf}\left(\frac{\partial v}{\partial z} + \frac{1}{r}\frac{\partial w}{\partial \phi}\right)_{z=0} \tag{14}$$

$$q_w = -k_{hnf}\left(1 + \frac{16\sigma^* T_\infty^3}{3k^* k}\right)\left(\frac{\partial T}{\partial z}\right)_{z=0}$$

Finally, the skin friction and Nusselt number are defines as follows:

$$Cf_r = \frac{\Omega_2}{\Omega_1}\sqrt{F'^2(0) + G'^2(0)}, Nu_r = -\frac{k_{hnf}}{k_f}\left(1 + \frac{4}{3}Rd\right)\Xi'(0) \tag{15}$$

The physical characteristics of hybrid nanofluid

$$\text{Dynamic viscosity} = \Omega_1 = \frac{\mu_{hnf}}{\mu_f} = \frac{1}{(1 - \Phi_1)^{2.5}(1 - \Phi_2)^{2.5}},$$

$$\text{Density} = \Omega_2 = \frac{\rho_{hnf}}{\rho_f} = (1 - \Phi_1)\left[(1 - \Phi_2) + \frac{\Phi_2 \rho_{2s}}{\rho_f}\right] + \frac{\Phi_1 \rho_{1s}}{\rho_f},$$

$$\text{Heat capacity} = \Omega_3 = \frac{(\rho c_p)_{hnf}}{(\rho c_p)_f} = (1 - \Phi_1)\left[(1 - \Phi_2) + \frac{\Phi_2(\rho c_p)_{2s}}{(\rho c_p)_f}\right] + \frac{\Phi_1(\rho c_p)_{1s}}{(\rho c_p)_f},$$

$$\text{Thermal conductivity} = \Omega_4 = \frac{k_{hnf}}{k_f} = \frac{k_{nf}}{k_f}\left(\frac{k_{s2} + 2k_{nf} - 2\Phi_2(k_{nf} - k_{s2})}{k_{s2} + 2k_{nf} + \Phi_2(k_{nf} - k_{s2})}\right),$$

3. Numerical procedure

This section uses the bvp4c shooting technique, which is written in MATLAB computational computer software, to solve the reduced ODEs (8–12) with associated boundary constraints (13). The Lobatto-IIIa collocation formula, which is utilized for numerical calculations, is the foundation of Bvp4c. By adding the following symbols, the multiple-order derivatives are transformed into first-order ODEs. The flow chart of bvp4c has been revealed in Fig. 2.

$$\Lambda_1 = F, \Lambda_2 = F', \Lambda_3 = G, \ \Lambda_4 = G', \ \Lambda_5 = H, \ \Lambda_6 = H', \ \Lambda_7 = \Xi, \ \Lambda_8 = \Xi'$$

then the reduced equations are framed out below form:

$$\Lambda_1' = \Lambda_2 \tag{16}$$

$$\Lambda_2' = \frac{\Omega_1}{\Omega_1}\left[\Lambda_1\,\Lambda_1 - \Lambda_3\,\Lambda_3 + \Lambda_5\,\Lambda_2 + \gamma\left(\Lambda_1 + \frac{\xi}{2}\Lambda_2\right)\right] - Fr\Lambda_1\Lambda_1 - \alpha_1\Lambda_1, \tag{17}$$

$$\Lambda_3' = \Lambda_4 \tag{18}$$

$$\Lambda_5' = -2\Lambda_1, \tag{19}$$

$$\Lambda_6' = \Lambda_7, \tag{20}$$

$$\Lambda_7' = \frac{\Omega_3\,Pr\left(\Lambda_5\Lambda_8 + \gamma\frac{\xi}{2}\Lambda_8\right)}{\left(\Omega_4 + \frac{4}{3}Rd\right)} \tag{21}$$

The appropriate boundary conditions are

$$\Lambda_1(0) = \Gamma + \Pi\Lambda_2(0), \Lambda_2(0) = \chi_1,\ \ \Lambda_3(0) = 1 + \Pi\Lambda_4(0), \tag{22}$$

$$\Lambda_4(0) = \chi_2, \Lambda_5(0) = 0, \Lambda_6(0) = \chi_3, \Lambda_7(0) = 1, \tag{23}$$

$$\Lambda_1(\infty) = 0,\ \Lambda_3(\infty) = 0,\ \Lambda_7(\infty) = 0. \tag{24}$$

After guessing the three unknowns, χ_1, χ_2, and χ_3, Bvp4c ran the whole numerical simulation until $F(\infty) = 0, G(\infty) = 0, \Xi(\infty) = 0$ were reached. Additionally, $\xi = \xi_\infty$ is used in place of the asymptotic boundary condition, which is at $\xi \to \infty$. In every instance, the inner iterative process is carried out with a convergence limit of 10^{-6}. Consequently, the complete solution is acquired.

4. Results and discussion

The present research attempts to comprehend the Darcy Forchheimer time-dependent flow of hybridized nanoparticles with thermal radiation due to slipping dis including its physical characteristics through heat transmission. Figs. 3–7 demonstrate the flow
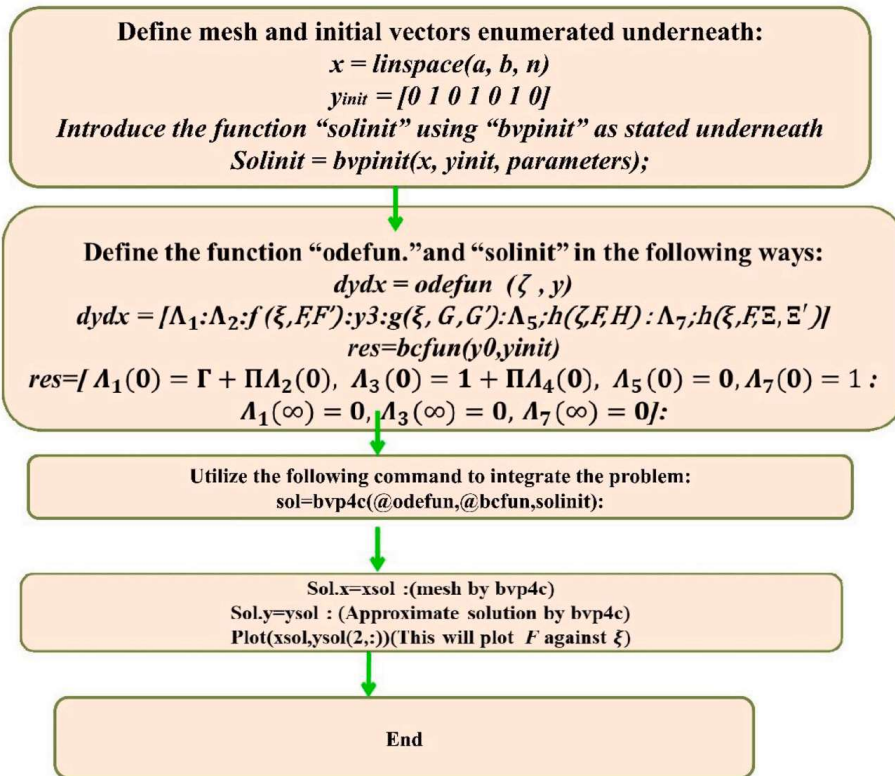

Fig. 2. Flow chart of Bvp4c.

behaviour against the radial velocity $F(\xi)$, azimuthal velocity $G(\xi)$, axial velocity $H(\xi)$ and temperature field $\Xi(\xi)$ associated physical characteristics. The physical dimensionless variables in the framework of conversion differential equations include the inertia coefficient ($0.1 \leq Fr \leq 0.9$), porosity effect ($0.1 \leq \alpha_1 \leq 0.9$), slip variable ($0.1 \leq \Pi \leq 1.0$), stretching variable ($0.1 \leq \Gamma \leq 0.5$), radiation variable ($0.1 \leq Rd \leq 0.5$), unsteady variable ($0.1 \leq \gamma \leq 0.5$), across the velocity distribution, temperature distribution, concentration of nanomaterial, motile density, entropy minimization and Bejan number. We used the following physical properties for demonstrating the framework: $Fr = 0.3$, $\alpha_1 = 0.9$, $\gamma = 0.2$, $Rd = 0.5$, $\Pi = 0.2$, $\Pi_1 = 0.02$, $\Pi_2 = 0.04$. It's worth noting all of the fields are progressively reaching far-field boundary conditions. The Prandtl number for the Kerosene Oil (KO) has been set for $Pr = 23.004$ with Hassain et al. [41]

Fig. 3(a)–3(c) demonstrates the effects of the inertia coefficient Fr on the velocity parameters of the radial velocity $F(\xi)$, azimuthal velocity $G(\xi)$, axial velocity $H(\xi)$ and their distributions for both the nanofluid (Ag/KO) and hybrid nanofluid cases ($Ag + GO/KO$). Fig. 3(a) provides a representation of the inertia coefficient Fr on the velocity parameters of the radial velocity $F(\xi)$ for the influence of the nanofluid (Ag/KO) and hybrid nanofluid cases ($Ag + GO/KO$). The visualization gives the impression that the larger in inertia coefficient Fr radial velocity $F(\xi)$ is lower. Permeability rises with increasing inertia coefficient Fr values, creating restriction in a fluid movement. Consequently, the fluid velocity is reduced. The influence of the inertia coefficient Fr for each of the nanofluid (Ag/KO) and hybrid nanofluid cases ($Ag + GO/KO$) across the azimuthal velocity $G(\xi)$ is exposed in Fig. 3(b). As we intensify the inertia coefficient Fr the across the azimuthal velocity $G(\xi)$ goes down, which is caused by the inertia coefficient Fr. The inertia coefficient Fr for the axial velocity $H(\xi)$ on nanofluid (Ag/KO) and hybrid nanofluid cases ($Ag + GO/KO$) is graphically exemplified in Fig. 3(c). It is evident that the axial velocity $H(\xi)$ begins to accelerate as the inertia coefficient Fr. Fig. 4(a–c) demonstrates the effects of porosity effect α_1 over the velocity parameters of the radial velocity $F(\xi)$, azimuthal velocity $G(\xi)$, axial velocity $H(\xi)$ through the nanofluid (Ag/KO) and hybrid nanofluid cases ($Ag + GO/KO$). Fig. 4(a) illustrates the radial velocity $F(\xi)$ for larger estimates of porosity effect α_1. the radial velocity $F(\xi)$ depreciates as the porosity effect α_1 enlarges. From this figure, hybrid nanofluid cases ($Ag + GO/KO$) exhibit superior behaviour to nanofluid nanofluid (Ag/KO). Physically, the existence of porous space causes an impediment in liquid flow, resulting in a diminution in radial velocity near the disk. Fig. 4(b) the azimuthal velocity $G(\xi)$ due the higher magnitude of porosity effect α_1 with nanofluid (Ag/KO) and hybrid nanofluid ($Ag + GO/KO$). An increase in azimuthal velocity $G(\xi)$ results in an reduction in azimuthal velocity (ξ). The effect of the porosity effect α_1 of nanofluid (Ag/KO) and hybrid nanofluid ($Ag + GO/KO$) across the axial velocity $H(\xi)$ is seen in Fig. 4(c). It has been reported that for nanofluid (Ag/KO) and hybrid nanofluid ($Ag + GO/KO$), the axial velocity $H(\xi)$ is improved for greater porosity effect α_1.
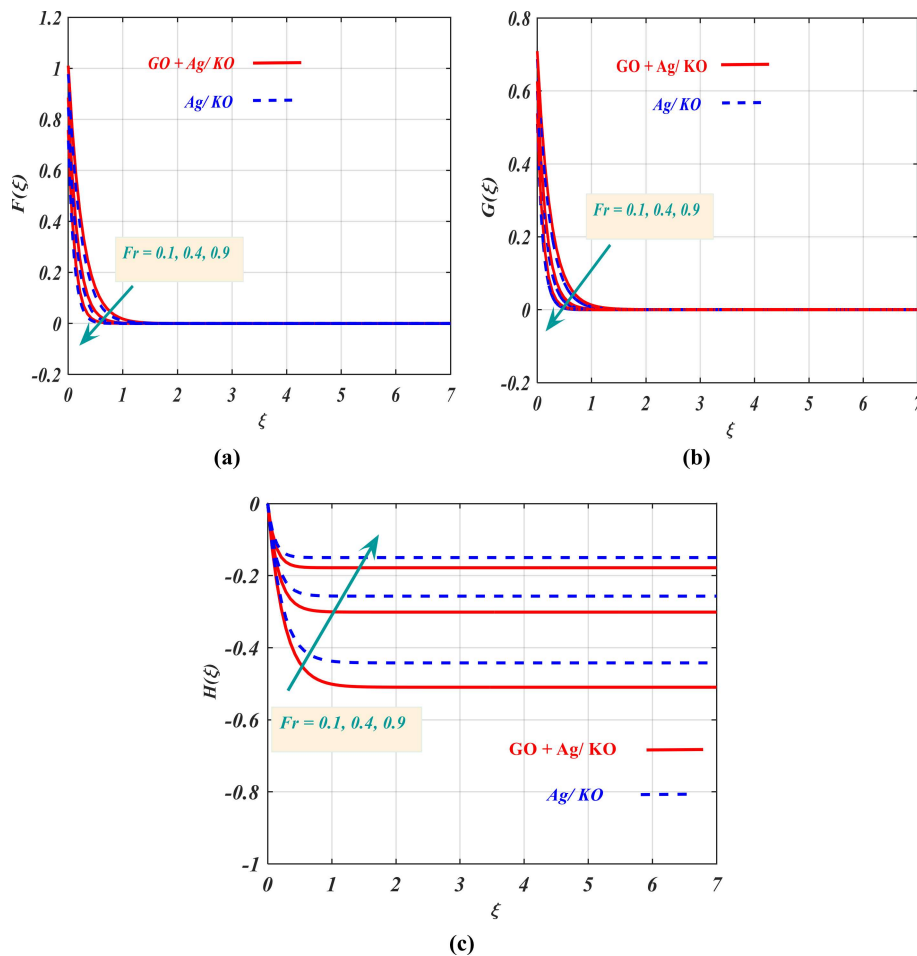

Fig. 3. Effect of inertia coefficient on (a) $F(\xi)$ (b) $G(\xi)$ (c) $H(\xi)$
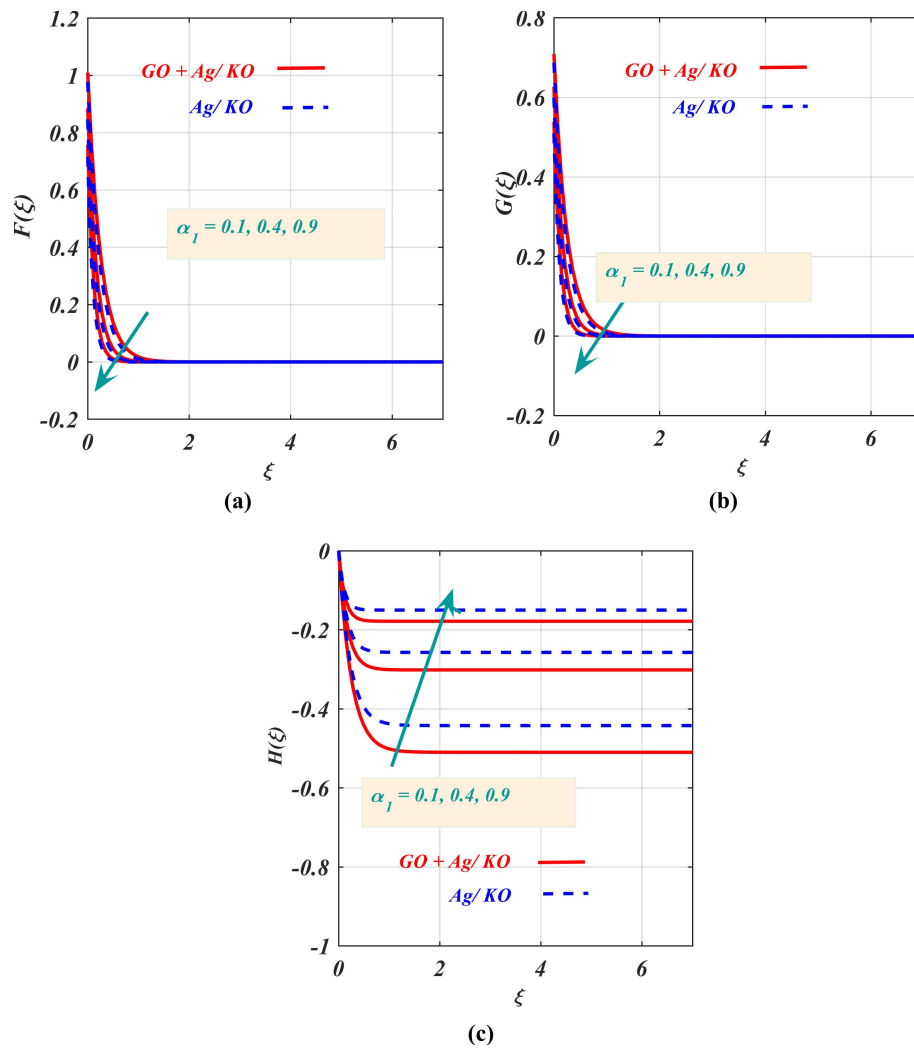
Fig. 4. Effect of porosity factor (a) $F(\xi)$ (b) $G(\xi)$ (c) $H(\xi)$

The plot of nanofluid (Ag/KO) and hybrid nanofluid ($Ag+GO/KO$) stretching variable Γ over the velocity parameters of the radial velocity $F(\xi)$, azimuthal velocity $G(\xi)$, axial velocity $H(\xi)$ has been exhibited in Fig. 5(a–c). Fig. 5(a) displays the results of stretching variable Γ across the radial velocity $F(\xi)$. The larger magnitude of the stretching variable Γ declines the radial velocity $F(\xi)$ of nanofluid (Ag/KO) and hybrid nanofluid ($Ag + GO/KO$). By changing how fluid constituents deform in the radial direction, the stretching parameter close to a revolving disk influences the radial velocity. Usually, a parameter controls how the liquid's radial velocity varies with disk distance, altering the properties of the outermost layer and the flow profile. The effects of stretching variable Γ versus the azimuthal velocity $G(\xi)$ are recognized in Fig. 5(b). Weak azimuthal velocity $G(\xi)$ are seen for higher estimations of stretching variable Γ in the presence of radial velocity $F(\xi)$ of nanofluid (Ag/KO) and hybrid nanofluid ($Ag + GO/KO$). Fig. 5(c) shows that for nanofluid (Ag/KO) and hybrid nanofluid ($Ag + GO/KO$), axial velocity $H(\xi)$ accelerates as stretching variable Γ rises. Fig. 6(a–c) compare the radial velocity $F(\xi)$, azimuthal velocity $G(\xi)$, axial velocity $H(\xi)$ of the nanofluid (Ag/KO) and hybrid nanofluid ($Ag+GO/KO$) under different values of Φ_1 and Φ_2. Fig. 6(a) views that for nanofluid (Ag/KO) and hybrid nanofluid ($Ag+GO/KO$) radial velocity $F(\xi)$ is an enhancing function of slip variable (Π). The slip effect around a revolving disk can alter the radial velocity of fluid in the region of the disk by lowering the resistance on the fluid and the appearance, thus alters the velocity profile. The type of substance, the viscosity of the fluid, and the slip duration all affect how much of a slip effect. Fig. 6(b) shows the slip variable (Π) trend on azimuthal velocity $G(\xi)$ for nanofluid (Ag/KO) and hybrid nanofluid ($Ag + GO/KO$). the azimuthal velocity $G(\xi)$ reduced as the slip variable (Π) enhanced. Fig. 6(c) indicates that axial velocity $H(\xi)$ decays due to the nanofluid (Ag/KO) and hybrid nanofluid ($Ag+GO/KO$) as the slip variable (Π) rises.

The impact of the thermal radiation Rd across the temperature field $\Xi(\xi)$ through the nanofluid (Ag/KO) and hybrid nanofluid ($Ag+GO/KO$) is illustrated in Fig. 7(a). The temperature field $\Xi(\xi)$ is growing with the rising magnitude of thermal radiation. Physically, it is evident from the relation between radiative thermal flow and Rosseland radiant absorptivity that, an increment in radiative thermal flow gives increment in the liquid's internal heat and an improvement in radiant heat conduction. As illustrated in Fig. 7(b), as the unsteady parameter γ becomes greater, the temperature field $\Xi(\xi)$ of the liquid flowing over the disk diminishes. For the nanofluid (Ag/KO) and hybrid nanofluid ($Ag+GO/KO$) nano-liquid categories.

The rate of heat transport and the factor of skin friction are the two most significant factors in thermal engineering. The drag
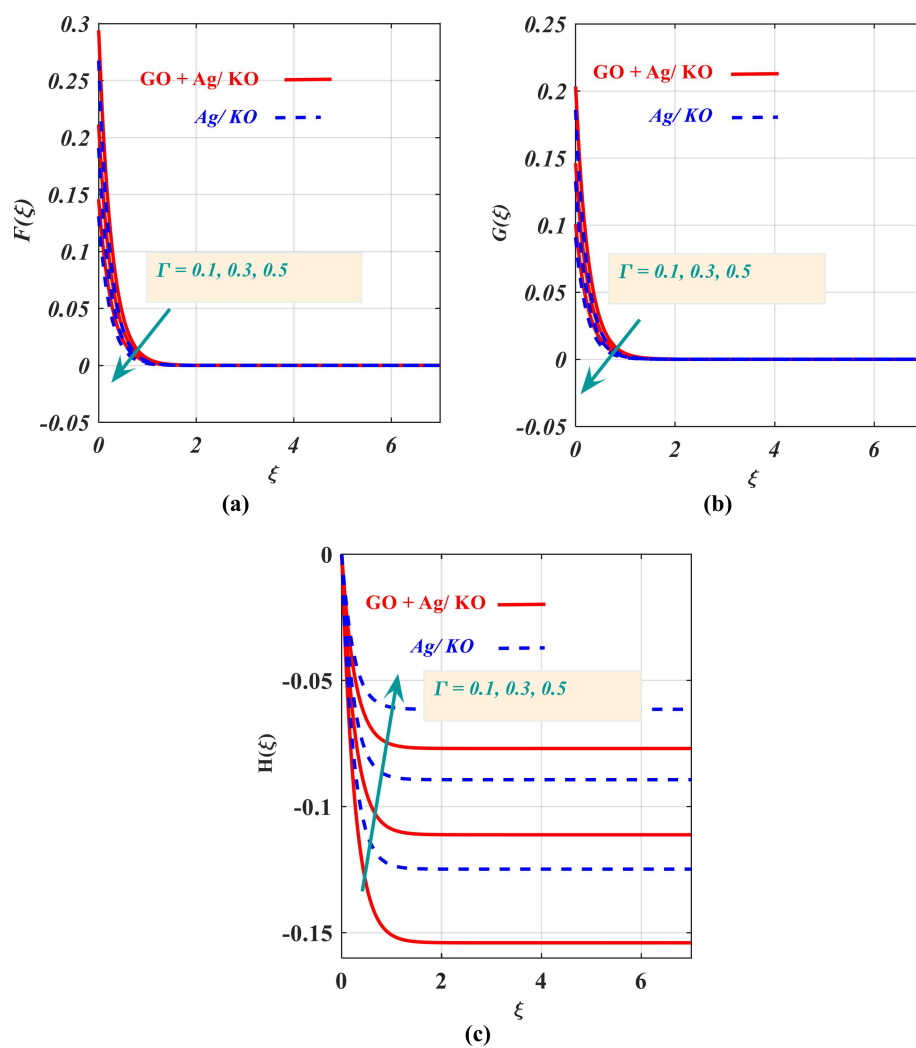
Fig. 5. Effect of stretching variable on (a) $F(\xi)$ (b) $G(\xi)$ (c) $H(\xi)$.
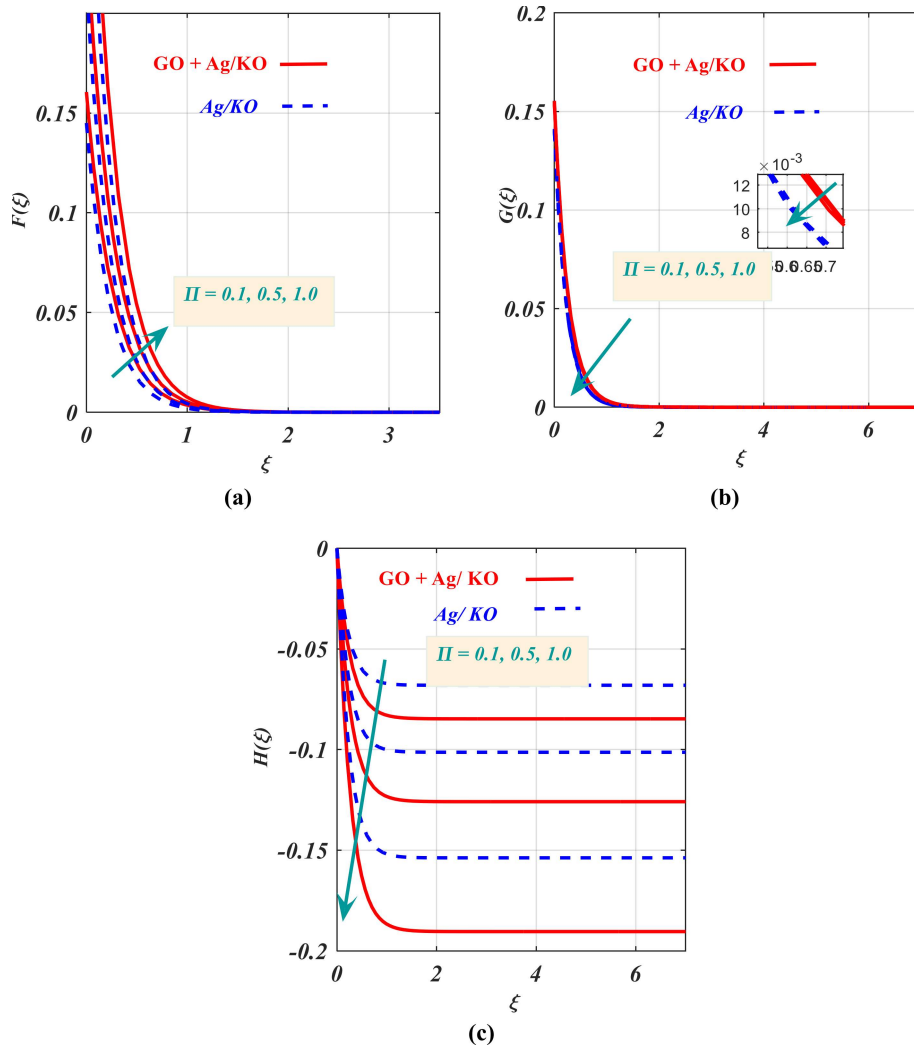
Fig. 6. Effect of slip parameter (a) $F(\xi)$ (b) $G(\xi)$ (c) $H(\xi)$
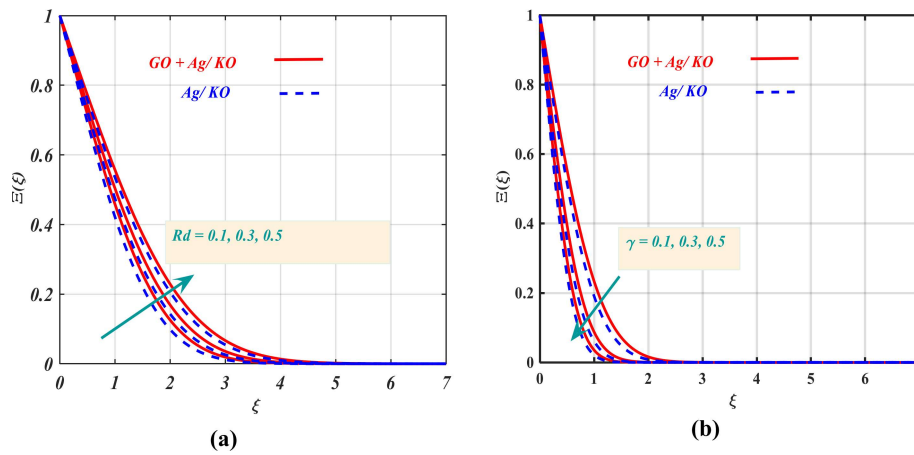

Fig. 7. (a–b): Effect of thermal radiation and unsteady variable on $\Xi(\xi)$.

friction Cf_r describes the drag force in liquid, while thermal diffusion rate is described by the Nusselt number Nu_r. Variations in Cf_r of the bar graph versus the stretching variable Γ are displayed in Fig. 8(a) which concerns two different fluid categories as nanofluid (Ag/KO) and hybrid nanofluid ($Ag+GO/KO$) respectively. As seen in the figures, the drag friction Cf_r depends on Γ. Fluctuation in heat transfer rate Nu_r versus the thermal radiation parameter is depicted in Fig. 8(b) concerning the nanofluid (Ag/KO) and hybrid nanofluid ($Ag+GO/KO$) categories. It is clear from this illustration that the heat diffusion rate is a rising function of Rd.
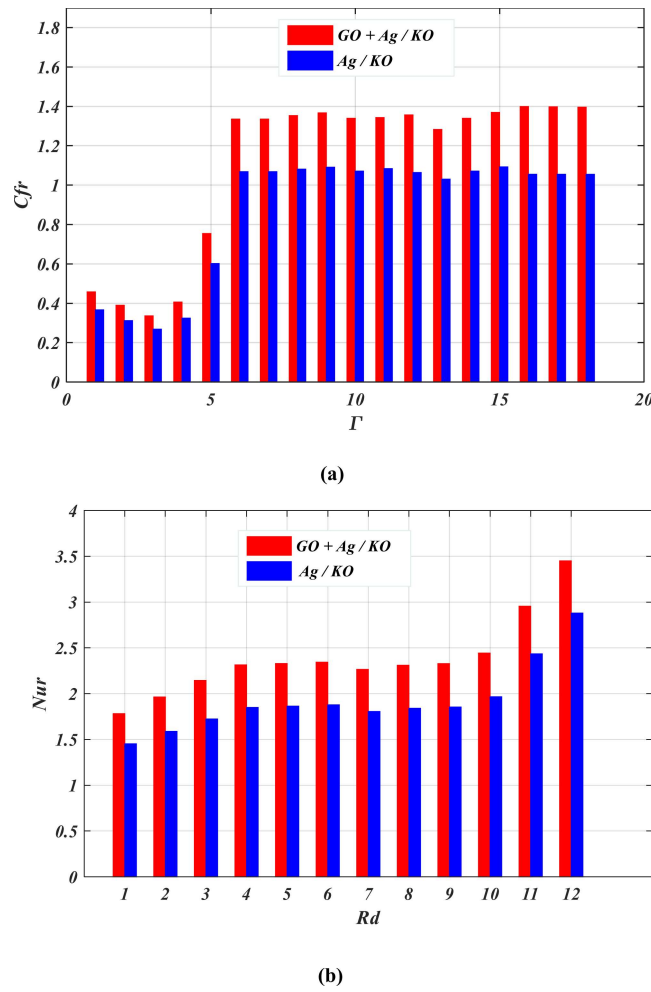
(a)

(b)

Fig. 8. (a) influence of Γ on *Cfr* **(b)** impact of *Rd* on *Nur*

Fig. 9(a) - 9(b) represents the influence of numerous factors on parameters drag friction Cf_r and Nusselt number Nu_r. Fig. 9(a) shows a three-dimensional representation of local skin friction as it varies with the parameter *Fr* and the porosity factor α_1. Fig. 9(b) shows the surface plot of Nusselt number Nu_r, in terms of the radiation parameter *Rd* and the unsteady parameter γ.

Additionally, Table 3 provide numerical values of drag friction Cf_r for the various magnitudes of porosity variable α_1, unsteady variable γ, inertia coefficient γ, slip factor Π, stretching variable Γ for the nanofluid (Ag/KO) and hybrid nanofluid ($Ag + GO/KO$). The larger magnitude of the porosity variable α_1 and stretching variable Γ reduces the drag friction Cf_r while enhancing the unsteady variable γ, inertia coefficient γ, slip factor Π. Consequently, it is discovered that the nanofluid (Ag/KO) and hybrid nanofluid ($Ag + GO/KO$) exhibit the most efficient behavior due the enhancement in the thermal radiation *Rd* and unsteady variable γ examined in Table 4. Finally, we compared our result with previous literature and it shows an outstanding agreement, which has been displayed in Table 5.

5. Conclusion

This study focused on analysing the influence of (Rd) and slip boundary conditions over transient Darcy–Forchheimer flow of ($GO + Ag/KO$) on a slippery rotating disk. By applying the similarity transformation technique, the non-linear PDEs are transformed into a set non-linear ODEs. Subsequently, the Bvp4c is implemented to approximate the resulting equations. Influence of multiple physical parameters on flow characteristics was examined using tables and graphs. The key findings are summarized as follows:

- As the parameters *Fr* and Γ increase, the tangential and radial velocity components for both nanofluid (Ag/KO) and hybrid nanofluid ($Ag + GO/KO$) nano-liquid case decreases.
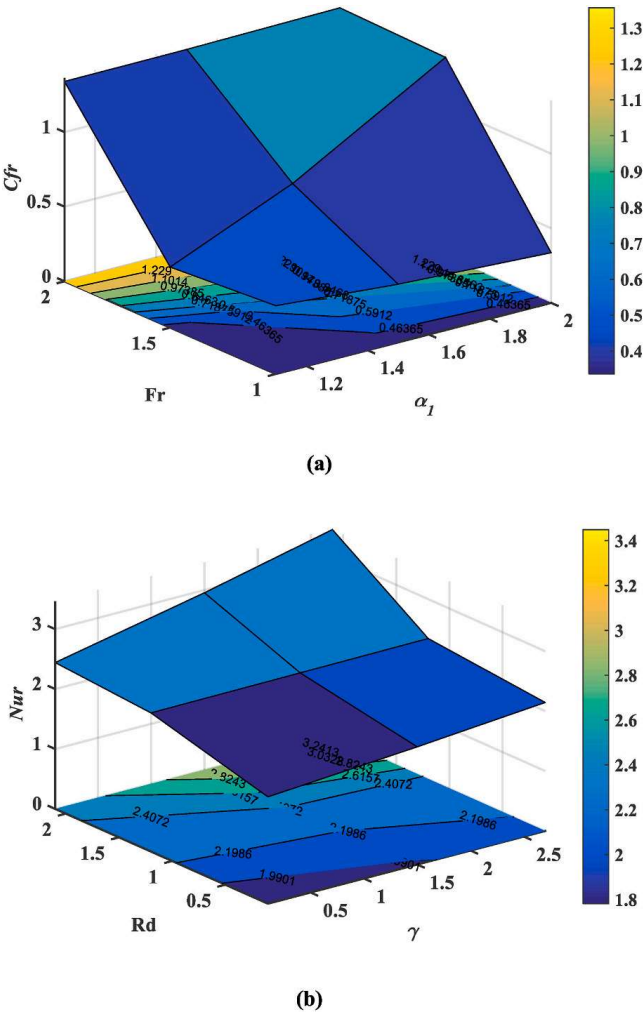
(a)

(b)

Fig. 9. 3D flow process **(a)** *Fr* and α_1 on *Cfr* **(b)** *Rd* and γ on (*Nur*)

Table 3
Numerical results of *Cfr* for various parameters.

					Cfr	
α_1	γ	*Fr*	Π	Γ	GO + Ag/KO	Ag/KO
1.1					0.4578	0.3667
1.2					0.3899	0.3119
1.3					0.3361	0.2685
	1.1				0.4061	0.3245
	1.5				0.7542	0.6018
	2.0				1.3352	1.0683
		1.0			1.3352	1.0683
		1.5			1.3530	1.0811
		2.0			1.3668	1.0909
			1.1		1.3192	1.0611
			1.2		1.3429	1.0838
			1.3		1.3565	1.9064
				0.1	1.3990	1.0550
				1.4	1.3876	1.0549
				2.7	1.3856	1.0548

- The axial velocity of the hybrid nanofluid increases with the porosity parameter and velocity slip parameter.
- As radiation *Rd* increases, the temperature of the kerosene oil-based hybrid nanofluid also increases, but a reverse relation is observed for the unsteadiness parameter.
- Skin friction profile is a rising function of the unsteadyness parameter, Darcy-Forchheimer number, and slip number.
- An enhancement in the porosity factor leads to a decrease in the distribution of skin friction Cf_r.

Table 4
Approximated Results of *Nur* for various parameter.

$\overline{Rd}$	$\overline{\gamma}$		*Nur*	
			GO + Ag/KO	Ag/KO
1.1			1.7815	1.4522
1.5			1.9633	1.5879
1.8			2.1440	1.7234
	1.0		2.3140	1.8493
	2.0		2.3287	1.8636
	3.0		2.3434	1.8779

Table 5
Comparison of Rd with drag friction and heat.

Rd	$F''(0)$	$\Xi'(0)$	$F''(0)$	$\Xi'(0)$
	Hussain et al. [39]		Current studies	
1	1.4159	0.7184	1.41592541	0.718414983
2	1.4452	0.8845	1.44525482	0.884524516

- The thermal transfer rate is elevated for greater thermal radiation parameter and unsteady parameters.

Nomenclature

u, v, w	Velocity component (m/s)
T_w	Temperature of the disk (K)
T_∞	Temperature away from the disk (K)
Fr	Inertia coefficient
Γ	Stretching parametr
Π	Slip parameter
Cf_r	Drag friction
Nu_r	Nusselt number
F	Dimensionless Radial velocity
G	Dimensionless Tangential velocity
H	Dimensionless Axial velocity
Ξ	Dimensionless temperature
Rd	Thermal radiation
Pr	Prandtl number
γ	Unsteady variable
Hybrid nanofliod	
$(c_p)_{hnf}$	Specific heat of hybrid nanofluid ($m^2/s^2 K$)
μ_{hnf}	Coefficient of viscosity (Kg/ms)
v_{hnf}	Kinematic viscosity of hybrid nanofluid (m^2/s)
ρ_{hnf}	Density of hybrid nanofluid (kg/m^{-3})
Nanofluid	
$(c_p)_{nf}$	Specific heat of hybrid nanofluid ($m^2/s^2 K$)
μ_{nf}	Coefficient of viscosity (Kg/ms)
v_{nf}	Kinematic viscosity of hybrid nanofluid (m^2/s)
ρ_{nf}	Density of hybrid nanofluid (kg/m^{-3})
k_{nf}	Thermal conductivity of hybrid nanofluid (Kgm/Ks^3)

CRediT authorship contribution statement

Zahoor Iqbal: Writing – original draft, Software, Methodology, Investigation, Conceptualization. **Farhan Ali:** Writing – original draft, Visualization, Software, Resources, Project administration. **Huiying Xu:** Software, Methodology, Conceptualization. **Xinzhong Zhu:** Validation, Software, Resources, Project administration, Funding acquisition, Formal analysis, Conceptualization. **M.M. Alqarni:** Software, Investigation, Formal analysis. **Arafat Hussain:** Writing – original draft, Software, Methodology, Investigation, Conceptualization. **Sharifah E. Alhazmi:** Formal analysis, Software, Visualization, Writing – review & editing. **Ehab M. Ragab:** Validation, Visualization, Writing – review & editing. **M. Faizan Ahmed:** Visualization, Investigation.

Declaration of competing interest

The authors declare that they have no known competing financial interests or personal relationships that could have appeared to

influence the work reported in this paper.

Acknowledgments

Data availability

No data was used for the research described in the article.

References

[1] T. Von Karman, Uber laminate und turbulent reibung Z, Angew Math Mech. 1 (1921) 233–252.

[2] S. Nadeem, M. Ijaz, M. Ayub, Darcy–Forchheimer flow under rotating disk and entropy generation with thermal radiation and heat source/sink, Journal of Thermal Analysis and Calorimetry 143 (2020) 2313–2328, https://doi.org/10.1007/s10973-020-09737-1.

[3] M.K. Nayak, A. Patra, S. Shaw, A. Misra, Entropy optimized Darcy-Forchheimer slip flow of Fe3O4−CH2OH2 nanofluid past a stretching/shrinking rotating disk, Heat Transfer 50 (2020) 2454–2487, https://doi.org/10.1002/htj.21987.

[4] Y. Chu, M.I. Khan, M.I.U. Rehman, S. Kadry, S. Qayyum, M. Waqas, Stability analysis and modeling for the three-dimensional Darcy-Forchheimer stagnation point nanofluid flow towards a moving surface, Appl. Math. Mech. 42 (2021) 357–370, https://doi.org/10.1007/s10483-021-2700-7.

[5] J.C. Umavathi, O.A. Bég, Computation of von Karman thermo-solutal swirling flow of a nanofluid over a rotating disk to a non-Darcian porous medium with hydrodynamic/thermal slip, Journal of Thermal Analysis and Calorimetry 147 (2021) 8445–8460, https://doi.org/10.1007/s10973-021-11126-1.

[6] B.K. Sharma, P. Sharma, N.K. Mishra, U. Fernandez-Gamiz, Darcy-Forchheimer hybrid nanofluid flow over the rotating Riga disk in the presence of chemical reaction: artificial neural network approach, Alex. Eng. J. 76 (2023) 101–130, https://doi.org/10.1016/j.aej.2023.06.014.

[7] F. Ali, M. Arif, M. Faizan, A. Saeed, T. Seangwattana, P. Kumam, A.M. Galal, Darcy Forchheimer flow of CMC-water based hybrid nanofluid due to a rotating stretchable disk, Heliyon 9 (2023) e17641, https://doi.org/10.1016/j.heliyon.2023.e17641.

[8] S. Nasir, W. Alghamdi, T. Gul, I. Ali, S. Sirisubtawee, A. Aamir, Comparative analysis of the hydrothermal features of TiO2 water and ethylene glycol-based nanofluid transportation over a radially stretchable disk, Numer. Heat Tran. Part B Fundamentals 83 (2023) 276–291, https://doi.org/10.1080/10407790.2023.2173343.

[9] S.U.S. Choi, Enhancing Thermal Conductivity of Fluids with Nanoparticles, ASME, 1995, p. 231. FED.

[10] E.E. M, E.M. Abedel-AaL, Darcy-forchheimer flow of a nanofluid over a porous plate with thermal radiation and Brownian motion, Journal of Nanofluids 12 (2022) 55–64, https://doi.org/10.1166/jon.2023.1910.

[11] J. Cui, A. Jan, U. Farooq, M. Hussain, W.A. Khan, Thermal analysis of radiative Darcy–Forchheimer nanofluid flow across an inclined stretching surface, Nanomaterials 12 (2022) 4291, https://doi.org/10.3390/nano12234291.

[12] S. Nasir, A.S. Berrouk, T. Gul, Analysis of chemical reactive nanofluid flow on stretching surface using numerical soft computing approach for thermal enhancement, Engineering Applications of Computational Fluid Mechanics 18 (2024), https://doi.org/10.1080/19942060.2024.2340609.

[13] F. Haider, T. Hayat, A. Alsaedi, Flow of hybrid nanofluid through Darcy-Forchheimer porous space with variable characteristics, Alex. Eng. J. 60 (2021) 3047–3056, https://doi.org/10.1016/j.aej.2021.01.021.

[14] S. Nasir, A.S. Berrouk, A. Aamir, Efficiency analysis of solar radiation on chemical radioactive nanofluid flow over a porous surface with magnetic field, Case Stud. Therm. Eng. (2024) 105231, https://doi.org/10.1016/j.csite.2024.105231.

[15] S. Eswaramoorthi, S. Nasir, K. Loganathan, M.S. Gupta, A. Berrouk, Numerical simulation of rotating flow of CNT nanofluids with thermal radiation, ohmic heating, and autocatalytic chemical reactions, Alex. Eng. J. 113 (2024) 535–550, https://doi.org/10.1016/j.aej.2024.10.124.

[16] S. Habib, S. Nasir, Z. Khan, A.S. Berrouk, N. Waseem, S. Islam, Machine learning-driven analysis of heat transfer in chemically reactive fluid flow considering soret-dufour effects, International Journal of Thermofluids 25 (2024) 100982, https://doi.org/10.1016/j.ijft.2024.100982.

[17] S. Nasir, Z. Shah, S. Islam, E. Bonyah, T. Gul, Darcy Forchheimer nanofluid thin film flow of SWCNTs and heat transfer analysis over an unsteady stretching sheet, AIP Adv. 9 (2019), https://doi.org/10.1063/1.5083972.

[18] A. Saeed, P. Kumam, S. Nasir, T. Gul, W. Kumam, Non-linear convective flow of the thin film nanofluid over an inclined stretching surface, Sci. Rep. 11 (2021), https://doi.org/10.1038/s41598-021-97576-x.

[19] G. Dharmaiah, S. Dinarvand, P. Durgaprasad, S. Noeiaghdam, Arrhenius activation energy of tangent hyperbolic nanofluid over a cone with radiation absorption, Results in Engineering 16 (2022) 100745, https://doi.org/10.1016/j.rineng.2022.100745.

[20] F. Ahmad, S. Abdal, H. Ayed, S. Hussain, S. Salim, A.O. Almatroud, The improved thermal efficiency of Maxwell hybrid nanofluid comprising of graphene oxide plus silver/kerosene oil over stretching sheet, Case Stud. Therm. Eng. 27 (2021) 101257.

[21] Z. Hussain, F. Aljuaydi, M. Ayaz, S. Islam, Enhancing thermal efficiency in MHD kerosene oil-based ternary hybrid nanofluid flow over a stretching sheet with convective boundary conditions, Results in Engineering 22 (2024) 102151.

[22] A. Zeeshan, M. Hassan, R. Ellahi, M. Nawaz, Shape effect of nanosize particles in unsteady mixed convection flow of nanofluid over disk with entropy generation, Proc. IME E J. Process Mech. Eng. 231 (4) (2017) 871–879.

[23] S. Nasir, S. Sirisubtawee, P. Juntharee, A.S. Berrouk, S. Mukhtar, T. Gul, Heat transport study of ternary hybrid nanofluid flow under magnetic dipole together with nonlinear thermal radiation, Appl. Nanosci. 12 (2022) 2777–2788, https://doi.org/10.1007/s13204-022-02583-7.

[24] A.S. Alnahdi, S. Nasir, T. Gul, Couple stress ternary hybrid nanofluid flow in a contraction channel by means of drug delivery function, Math. Comput. Simulat. 210 (2023) 103–119, https://doi.org/10.1016/j.matcom.2023.02.021.

[25] S. Nasir, A.S. Berrouk, T. Gul, I. Zari, Chemically radioactive unsteady nonlinear convective couple stress Casson hybrid nanofluid flow over a gyrating sphere, Journal of Thermal Analysis and Calorimetry 148 (2023) 12583–12595, https://doi.org/10.1007/s10973-023-12608-0.

[26] M. Behrouz, S. Dinarvand, M.E. Yazdi, H. Tamim, I. Pop, A.J. Chamkha, Mass-based hybridity model for thermomicropolar binary nanofluid flow: first derivation of angular momentum equation, Chin. J. Phys. 83 (2023) 165–184, https://doi.org/10.1016/j.cjph.2023.03.006.

[27] S. Dinarvand, H. Berrehal, H. Tamim, G. Sowmya, S. Noeiaghdam, M. Abdollahzadeh, Squeezing flow of aqueous CNTs-Fe3O4 hybrid nanofluid through mass-based approach: effect of heat source/sink, nanoparticle shape, and an oblique magnetic field, Results in Engineering 17 (2023) 100976, https://doi.org/10.1016/j.rineng.2023.100976.

[28] H. Berrehal, S. Dinarvand, I. Khan, Mass-based hybrid nanofluid model for entropy generation analysis of flow upon a convectively-warmed moving wedge, Chin. J. Phys. 77 (2022) 2603–2616, https://doi.org/10.1016/j.cjph.2022.04.017.

[29] S. Dinarvand, M. Behrouz, S. Ahmadi, P. Ghasemi, S. Noeiaghdam, U. Fernandez-Gamiz, Mixed convection of thermomicropolar AgNPs-GrNPs nanofluid: an application of mass-based hybrid nanofluid model, Case Stud. Therm. Eng. 49 (2023) 103224, https://doi.org/10.1016/j.csite.2023.103224.

[30] T.H. Al-arabi, M.R. Eid, R.D. Alsemiry, S.A. Alharbi, R. Allogmany, E.M. Elsaid, Electromagnetic and Darcy-Forchheimer porous model effects on hybrid nanofluid flow in conical zone of rotatable cone and expandable disc, Alex. Eng. J. 96 (2024) 206–217.

[31] M. Alhadri, J. Raza, U. Yashkun, L.A. Lund, C. Maatki, S.U. Khan, L. Kolsi, Response surface methodology (RSM) and artificial neural network (ANN) simulations for thermal flow hybrid nanofluid flow with Darcy-Forchheimer effects, J. Indian Chem. Soc. 99 (8) (2022 Aug 1) 100607.

[32] S. Nasir, A. Berrouk, A. Aamir, Exploring nanoparticle dynamics in binary chemical reactions within magnetized porous media: a computational analysis, Sci. Rep. 14 (2024), https://doi.org/10.1038/s41598-024-76757-4.

[33] A.K. Alzahrani, M.Z. Ullah, A.S. Alshomrani, T. Gul, Hybrid nanofluid flow in a Darcy-Forchheimer permeable medium over a flat plate due to solar radiation, Case Stud. Therm. Eng. 26 (2021) 100955.

[34] F. Ali, A. Zaib, T. Padmavathi, M. Faizan, S.S. Zafar, Exact solution of radiative flow on the mixed convection flow of Hybrid Nanofluid in a porous medium; Laplace transform technique for sustainable energy, Surf. Rev. Lett. (2024), https://doi.org/10.1142/s0218625x25501161.

[35] S. Nasir, S. Islam, T. Gul, Z. Shah, M.A. Khan, W. Khan, A.Z. Khan, S. Khan, Three-dimensional Rotating Flow of MHD Single Wall Carbon Nanotubes over a Stretching Sheet.

[36] L.A. Lund, M.A. Fadhel, S. Dero, Z. Shah, M. Alsheri, A. Alshehri, Slip and radiative effect on magnetized CNTs/C2H6O2+ H2O hybrid base nanofluid over exponentially shrinking surface, J. Magn. Magn Mater. 580 (2023) 170958.

[37] N. Acharya, S. Maity, P.K. Kundu, Entropy generation optimization of unsteady radiative hybrid nanofluid flow over a slippery spinning disk, Proc. IME C J. Mech. Eng. Sci. 236 (11) (2022) 6007–6024.

[38] M.M. Rahman, I.A. Eltayeb, Convective slip flow of rarefied fluids over a wedge with thermal jump and variable transport properties, Int. J. Therm. Sci. 50 (4) (2011) 468–479.

[39] Z. Hussain, F. Aljuaydi, M. Ayaz, S. Islam, Enhancing thermal efficiency in MHD kerosene oil-based ternary hybrid nanofluid flow over a stretching sheet with convective boundary conditions, Results in Engineering 22 (2024) 102151, https://doi.org/10.1016/j.rineng.2024.102151.